

# Tuning the Local Availability of VEGF within Glycosaminoglycan-Based Hydrogels to Modulate Vascular Endothelial Cell Morphogenesis

Yanuar Dwi Putra Limasale, Passant Atallah, Carsten Werner,\* Uwe Freudenberg, and Ralf Zimmermann\*

Incorporation of sulfated glycosaminoglycans (GAGs) into cell-instructive polymer networks is shown to be instrumental in controlling the diffusivity and activity of growth factors. However, a subtle balance between local retention and release of the factors is needed to effectively direct cell fate decisions. To quantitatively unravel material characteristics governing these key features, the GAG content and the GAG sulfation pattern of star-shaped poly(ethylene glycol) (starPEG)–GAG hydrogels are herein tuned to control the local availability and bioactivity of GAG-affine vascular endothelial growth factor (VEGF165). Hydrogels containing varying concentrations of heparin or heparin derivatives with different sulfation pattern are prepared and thoroughly characterized for swelling, mechanical properties, and growth factor transport. Mathematical models are developed to predict the local concentration and spatial distribution of free and bound VEGF165 within the gel matrices. The results of simulation and experimental studies concordantly reveal how the GAG concentration and sulfation pattern determine the local availability of VEGF165 within the cell-instructive hydrogels and how the factor—in interplay with cell-instructive gel properties—determines the formation and spatial organization of capillary networks of embedded human vascular endothelial cells. Taken together, this study exemplifies how mathematical modeling and rational hydrogel design can be combined to pave the way for precision tissue engineering.

## 1. Introduction

Engineering living matter often requires the integration of cellular components into biomaterial scaffolds together with the provision of soluble signaling molecules such as growth factors and cytokines.<sup>[1]</sup> However, controlling the spatiotemporal availability, as well as the activity of the signaling molecules within engineered tissue constructs, remains challenging.<sup>[2]</sup> Incorporation of sulfated glycosaminoglycans (GAGs) in biomaterials offers a powerful means to modulate the distribution and stability of growth factors and cytokines due to the—mainly electrostatically controlled—complexation of the highly anionic GAGs with the signaling proteins through their positively charged surface domains. Accordingly, GAG-based hydrogels have been previously applied as cell-instructive matrices to control, for example, the morphogenesis of human vascular endothelial cells and kidney tubule cells as well as the fate of early hematopoietic progenitor cells in 3D cultures offering thoroughly defined exogenous cues.<sup>[1a,3]</sup> In these systems, the customization of the gel matrices for the presentation of specific


combinations of soluble signaling molecules was accompanied by the adjustment of the materials for their mechanical properties, cell adhesiveness, and susceptibility for enzymatic cleavage.

Targeting cellular fate control and functionality by the administration of soluble signaling molecules through engineered biomaterials requires a subtle balance between their localized retention and delivery to embedded cells. For GAG-based gels, this is governed by the GAG content, i.e., the volume density of binding sites and the affinity of the GAG to signaling molecules, i.e., the specific sulfation pattern.<sup>[4]</sup> To quantitatively unravel the role of these parameters on the local availability of signaling molecules in general and the proangiogenic vascular endothelial growth factor (VEGF165) in particular, we herein exploited a tunable cell-instructive hydrogel platform based on heparin (derivatives) and 4-arm star-shaped poly(ethylene glycol) (starPEG) peptide conjugates covalently crosslinked by a Michael type addition scheme (Figure 1).<sup>[5]</sup>

The approach refers to a recent own study in which the heparin concentration and the heparin (derivative) sulfation

Y. D. P. Limasale, Dr. P. Atallah, Prof. C. Werner, Dr. U. Freudenberg, Dr. R. Zimmermann  
Leibniz Institute of Polymer Research Dresden (IPF)  
Max Bergmann Center of Biomaterials Dresden (MBC)  
Hohe Str. 6, Dresden 01069, Germany  
E-mail: carsten.werner@tu-dresden.de; zimmermn@ipfdd.de

Prof. C. Werner  
Technische Universität Dresden  
Center of Regenerative Therapies Dresden (CRTD) and Cluster of Excellence Physics of Life (PoL)  
Dresden 01062, Germany

 The ORCID identification number(s) for the author(s) of this article can be found under <https://doi.org/10.1002/adfm.202000068>.

© 2020 The Authors. Published by WILEY-VCH Verlag GmbH & Co. KGaA, Weinheim. This is an open access article under the terms of the Creative Commons Attribution License, which permits use, distribution and reproduction in any medium, provided the original work is properly cited.

DOI: 10.1002/adfm.202000068

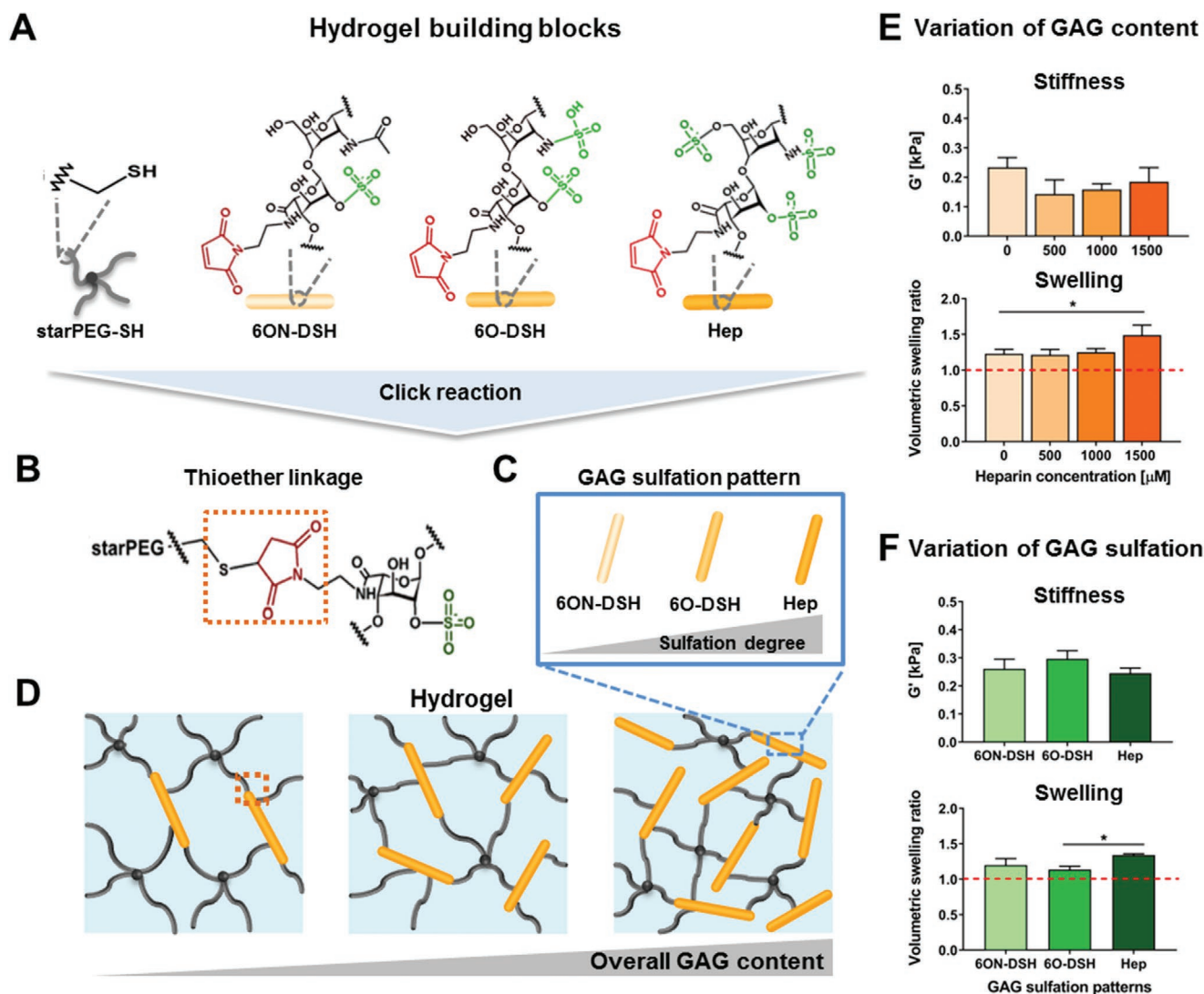


**Figure 1.** Formation and physical characterization of biohybrid starPEG-GAG hydrogels with adjustable GAG concentration and GAG sulfation pattern. A) The hydrogels were formed from thiol-functionalized starPEG (starPEG-SH), and maleimide functionalized heparin (Hep)/heparin derivatives, which were selectively desulfated at 6O- (6O-DSH), or 6O- and N-position (6ON-DSH). B) The starPEG-SH can be instantaneously reacted with maleimide-functionalized heparin/heparin derivatives to form a hydrogel network containing a stable thioether linkage. C) Variation in the local sulfate density of the hydrogel can be achieved by incorporating heparin/heparin derivatives with different sulfation patterns. D) The overall GAG content of the hydrogel can also be adjusted by changing the solid content and crosslinking degree (molar ratio of starPEG to GAG) of the hydrogels. E) Stiffness and volumetric swelling of the GAG hydrogel with a varied GAG content. F) Stiffness and volumetric swelling of the hydrogel with different GAG sulfation patterns. Data are presented as mean  $\pm$  SD for  $n = 3$ ,  $*P < 0.05$ .

pattern of binary biohybrid hydrogels have been systematically varied to tailor both the integral space charge density of the polymer networks and the local charge density of the GAG component to explore the relevance of these features for the sequestration of various cytokines, chemokines, and growth factors.<sup>[6]</sup> Moreover, starPEG-heparin hydrogels were successfully applied in earlier studies for embedding human umbilical vein endothelial cells (HUVECs) to create a versatile and robust 3D in vitro model of angiogenesis.<sup>[1a]</sup> Since VEGF plays a vital role in the early regulation of angiogenesis,<sup>[7]</sup> controlling the availability of free and active VEGF within the hydrogel materials is critically important to direct the tubular morphogenesis of endothelial cells.

Our reported study built on an unprecedentedly broad variation of GAG-hydrogel-parameters and quantified their relevance for the interaction of the gels with various signaling molecules of different physicochemical properties. A mathematical model for the prediction of the local concentration and spatial distribution of free and bound VEGF165 within the gel matrix variants was developed and experimentally validated. The availability of free VEGF165 was demonstrated to be decisive for the morphogenesis of gel-embedded human vascular endothelial cells to form capillary networks, and the administration of the factor by a microfluidic set-up was accordingly shown to direct the spatial organization of the emerging capillary structures.

## 2. Results

### 2.1. Basic Properties of Modular starPEG-GAG Hydrogels

In order to modulate the affinity of the hydrogel for a given signaling molecule, hydrogels were formed from heparin (derivatives) of varied sulfation degree or with variable heparin (derivative) concentration in the swollen polymer networks using a biorthogonal Michael-type addition crosslinking reaction (Figure 1A–D). Heparin (Hep) was regioselectively desulfated at the 6O- position to generate 6O-desulfated heparin (6O-DSH), or both at 6O- and N-positions to synthesize 6ON-desulfated heparin (6ON-DSH) as previously described (Figure 1A).<sup>[4]</sup> This strategy enabled the generation of heparin derivatives with a sulfation degree of  $\approx 67\%$  and  $\approx 33\%$  relative to the fully sulfated heparin (Hep), respectively. The percentages (%) of sulfation have been calculated based on the assumption that our heparin consists only of the well known major sequence with one 6O-, one N-, and one 2O-sulfate group present per disaccharide unit (corresponding to 100% sulfation degree),<sup>[8]</sup> and that the desulfation procedure produces heparin derivatives with quantitative removal of the particular 6O- or N-sulfate sulfate groups based on the procedures established by Attallah et al.<sup>[4]</sup> Subsequent functionalization of the Hep or its desulfated derivatives with maleimide moieties further allowed for crosslinking with thiol-terminated starPEG through a Michael type addition reaction scheme to form a stable thioether in the presence of biofluids (Figure 1B). Due to the specificity of the reaction, the crosslinking reaction is also compatible with the embedding of cells and various growth factors loading during the gel formation.

The heparin (derivative) concentration of the gels has been tuned by adjusting the overall solid content of the conjugate solutions (Figure 1D), whereas the local GAG sulfation pattern can be adjusted by the choice of the heparin (derivative) (Figure 1C). As the formation of capillary structures of HUVECs can be achieved in soft starPEG-heparin hydrogels of a storage modulus of  $\approx 200$  Pa only,<sup>[1a]</sup> the effect of heparin (derivative) content and the heparin (derivative) sulfation pattern on the diffusivity of signaling molecules, the release of VEGF, and the HUVECs morphogenesis were investigated using a set of gel variants of this stiffness range (Figure 1E–F).

For investigating the effect of GAG content on the transport and the bioactivity of the VEGF within the scaffold, a set of hydrogels containing fully sulfated heparin was produced with a total heparin concentration in the range of  $(500\text{--}1500) \times 10^{-6}$  M (Figure 1E). Furthermore, a heparin-free PEG hydrogel was used as control. By adjusting the overall solid content in the range from 2% to 4% (for varying molar ratios of starPEG to heparin) we could prepare hydrogels with a similar stiffness of  $\approx 200$  Pa. Volume swelling measurements in phosphate-buffered saline (PBS) of all hydrogels indicated an increase in swelling of less than 30% from its original volume upon hydrogel synthesis, with the highest swelling was observed for the hydrogels prepared with the highest heparin concentration ( $1500 \times 10^{-6}$  M) (Figure 1E).

Next, in order to understand the effect of the GAG affinity on the bioactivity of administered VEGF, hydrogels containing fully sulfated heparin (starPEG-Hep), 6O-desulfated

heparin (starPEG-6O-DSH), and 6ON desulfated heparin (starPEG-6ON-DSH) were prepared at similar heparin concentration of  $1500 \times 10^{-6}$  M (Figure 1F). Hydrogels with variable GAG sulfation patterns were produced with similar mechanical properties of  $\approx 200$  Pa by altering the GAG variant while keeping the total GAG content as well as the molar ratio of starPEG to GAG constant (Figure 1F). Interestingly, similar to the hydrogels prepared with a low heparin content (Figure 1E), a slightly lower volume swelling ratio was observed within the hydrogels containing GAG building blocks with a lower sulfation degree compared to the fully sulfated heparin (Figure 1E,F). These results can be attributed to the decrease in the osmotic hydrogel expansion forces due to the reduced number of sulfate groups present in the polymer networks.<sup>[8]</sup>

### 2.2. Mobility of Soluble Signaling Molecules in starPEG-GAG Hydrogels of Varied GAG Content and Sulfation Patterns

The mobility of signaling molecules with different GAG-affinity and different dimensions across the set of starPEG-GAG hydrogel variants was studied (Table S1, Supporting Information). Four proteins were chosen to represent small and large signaling molecules with a strong affinity to heparin (stromal cell-derived factor 1 $\alpha$  (SDF1 $\alpha$ ) and VEGF165) and with almost no affinity to heparin (epidermal growth factor (EGF) and VEGF121). As the basis for these studies, we prepared a set of hydrogels with variation in the heparin (derivative) concentration and sulfation pattern, whereas the stiffness of all gels was adjusted to  $\approx 200$  Pa. Applying the rubber elasticity theory,<sup>[9]</sup> the mesh size of the hydrogels was estimated to be  $\approx 30$  nm (Table S2, Supporting Information), which is significantly larger than the hydrodynamic radius of the proteins used in this study. The mobility of signaling molecules within an affinity-based system that allows for a reversible binding, such as a GAG-based hydrogel system, can be described by their effective diffusion coefficient,  $D$ .<sup>[10]</sup> To determine  $D$  for the proteins used in this study, we applied the fluorescence recovery after photobleaching (FRAP) technique (Figure 2).

First, the diffusion coefficients of four different proteins have been determined for hydrogels with graded heparin concentration (Figure 2A). The analysis revealed a similar diffusivity of the nonaffine proteins within the hydrogels with graded heparin content. The magnitude of the diffusion coefficients was found to be inversely correlated to their molecular size ( $\approx 20$  and  $60 \mu\text{m}^2 \text{s}^{-1}$ , for large and small nonaffine proteins, respectively) (Figure 2A). On the other hand, the diffusivity of the heparin-affine proteins was significantly reduced in heparin-containing gels (Figure 2A). For SDF1 $\alpha$ , the diffusion coefficient decreased from  $\approx 80 \mu\text{m}^2 \text{s}^{-1}$  in the pure PEG hydrogel to  $\approx 15 \mu\text{m}^2 \text{s}^{-1}$  or lower ( $\leq 5$  factors) in the heparin-containing hydrogels. A similar trend was also observed for the larger heparin-binding protein, VEGF165. Here, the mobility of the protein decreased by a factor of  $\approx 2.5$  if a starPEG-Hep hydrogel with a concentration of  $500 \times 10^{-6}$  M heparin was compared to a pure PEG hydrogel. Moreover, the adjustment of the heparin concentration from  $500 \times 10^{-6}$  to  $1500 \times 10^{-6}$  M within the starPEG-Hep hydrogels further decreased the effective diffusion coefficient of the heparin-affine proteins, whereas the corresponding value of the

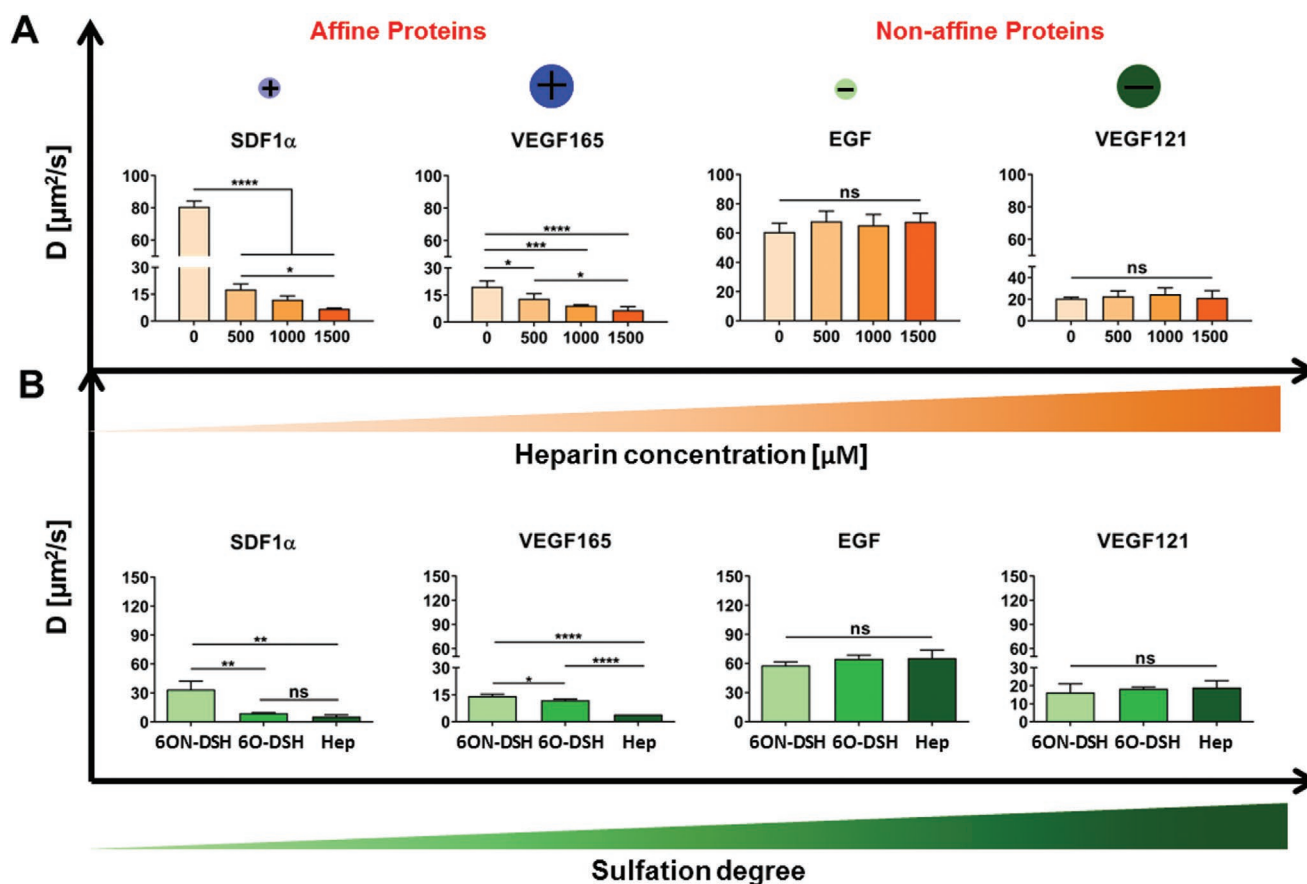


**Figure 2.** GAG content and sulfation pattern govern the transport of heparin-affine proteins in starPEG-GAG hydrogels. A) Influence of the heparin concentration on the diffusivity of heparin-affine proteins (SDF1 $\alpha$  and VEGF165) and nonaffine proteins (EGF and VEGF121) in starPEG-Hep hydrogels with a total heparin concentration of 0, 500, 1000, and 1500  $\times 10^{-6}$  M. B) Effect of the heparin derivative sulfation pattern on the diffusivity of heparin-affine and nonaffine proteins (same as in panel (A)). For this, the effective diffusion coefficient of the proteins was investigated in starPEG-6ON-DSH, starPEG-6O-DSH, starPEG-Hep hydrogels with an overall heparin concentration of 1500  $\times 10^{-6}$  M by FRAP. Data are presented as mean  $\pm$  SD for  $n = 3$ , “ns” stands for not significant, \* $P < 0.05$ , \*\* $P < 0.01$ , \*\*\* $P < 0.001$ , and \*\*\*\* $P < 0.0001$ .

small or large nonaffine proteins (EGF and VEGF121, respectively) was not affected (Figure 2A).

Next, we extended our analysis on the mobility of the signaling molecules in the hydrogel with varied heparin derivative sulfation patterns including hydrogels made of fully sulfated heparin (starPEG-Hep hydrogel, 100% sulfation degree), the 6O-desulfated heparin (derivative) (starPEG-6O-DSH hydrogel, 67% sulfation degree) and the 6ON-desulfated heparin (derivative) (starPEG-6ON-DSH hydrogels, 33% sulfation degree (Figure 2B)). In general, the diffusivity of nonaffine proteins (EGF and VEGF121) within the hydrogels was not affected by the heparin derivative sulfation pattern. In this case, diffusion is controlled primarily by the molecular weight of the proteins (Table S1, Supporting Information). Accordingly, the diffusion coefficient of the smaller EGF was found to be  $\approx 60 \mu\text{m}^2 \text{s}^{-1}$ , whereas the corresponding value of the larger VEGF121 was  $\approx 18 \mu\text{m}^2 \text{s}^{-1}$ . In contrast, the diffusivity of the heparin affine proteins was inversely correlated to the GAG sulfation degree (Figure 2B) and dependent on the presence of specific sulfate groups. The diffusion coefficient of SDF1- $\alpha$  in the starPEG-6O-DSH hydrogel was not significantly different compared to that in the hydrogel prepared with the fully sulfated heparin. In contrast to this, the diffusivity of SDF1- $\alpha$

significantly increased from  $\approx 9 \mu\text{m}^2 \text{s}^{-1}$  in the starPEG-Hep hydrogel (100% sulfation degree) to  $\approx 30 \mu\text{m}^2 \text{s}^{-1}$  in starPEG-6ON-DSH hydrogels (33% sulfation degree, see Figure 2B), suggesting the critical role of N-sulfate group in determining the binding of SDF1- $\alpha$  to the heparin. Interestingly, the 6O and N sulfate group of heparin affected the diffusivity of VEGF165 differently compared to those on the SDF1- $\alpha$ . VEGF165 diffused nearly 3-fold faster in the starPEG-6O-DSH (67% sulfation degree, Figure 2B) gel compared to that in the starPEG-Hep gel, and the value increased further in starPEG-6ON-DSH gel with 33% sulfation degree.

The determined impact of the GAG concentration and sulfation pattern of the hydrogel on the in-gel diffusivity of the heparin-affine proteins VEGF165 and SDF1 $\alpha$  might be influenced by the presence of a specific heparin-binding site. However, our FRAP analysis of the diffusion of thrombin (Table S1, Supporting Information), a positively charged protein that interacts with heparin nonspecifically,<sup>[11]</sup> revealed similar correlations between both parameters and the diffusivity in the gel (Figure S3, Supporting Information).

Finally, we investigated the effect of protein's molecular weight and the mesh size of the hydrogel on the diffusivity of different model proteins within the hydrogels. Our studies revealed

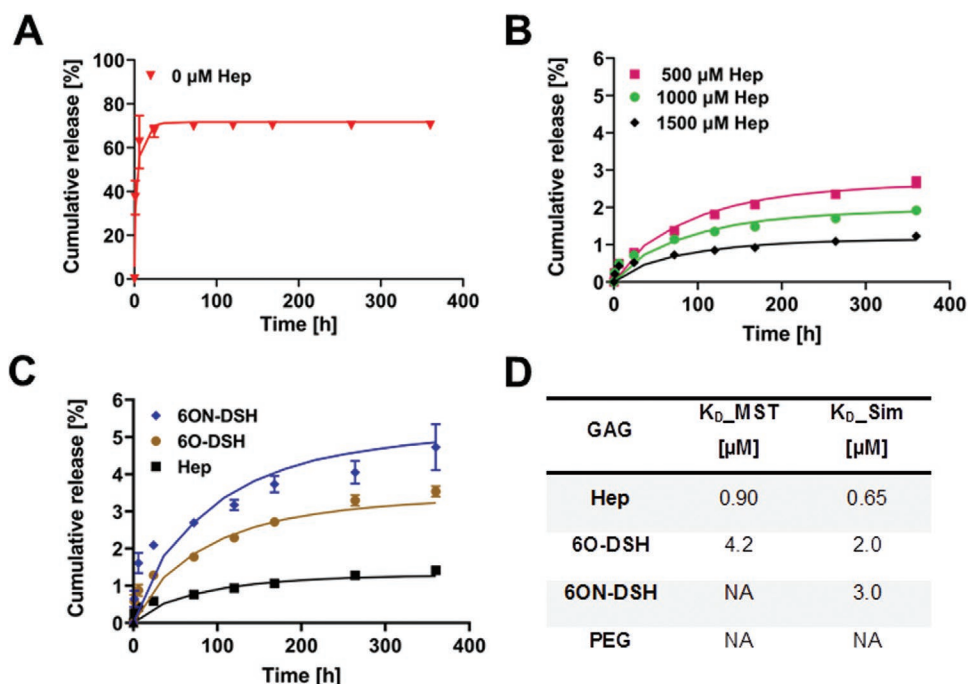


**Figure 3.** GAG content and sulfation pattern determine the release of VEGF165 from starPEG-GAG hydrogels. A) VEGF165 release from nonaffine PEG hydrogel. B) VEGF165 release from hydrogels with varying heparin concentration. C) VEGF165 release from hydrogels containing heparin derivatives with different sulfation patterns. The release experiment was conducted at 37 °C in endothelial cell growth medium (ECGM) supplemented with 0.1% BSA over 360 h. The data points represent experimental data (mean  $\pm$  SD for  $n \geq 3$ ) and the solid lines, fit curves obtained from the reaction–diffusion model. D) Comparison between the binding constant of the VEGF to the GAGs obtained from the microscale thermophoresis and the curve fitting of the experimental release.

that the molecular weight significantly affected the diffusivity of the nonaffine proteins in pure PEG gels and heparin-containing gels, with the diffusion coefficient inversely correlated to the protein size (Figure S4, Supporting Information). In contrast, the molecular weight of the proteins minimally affected the diffusivity of heparin-affine proteins in starPEG-Hep hydrogels but strongly influenced their diffusion in pure (nonaffine) PEG hydrogels. Similarly, we observed an influence of the hydrogel mesh size on the transport of nonaffine proteins but not for heparin-affine proteins. The small or large nonaffine proteins diffused significantly faster with an increasing mesh size of the hydrogels, whereas the in-gel diffusivity of the affine proteins remained unaffected (Figure S5, Supporting Information).

Overall, both the GAG content as well as the GAG sulfation pattern modulate the in-gel diffusivity of the heparin-affine proteins, whereas the diffusivity of the nonaffine proteins remained similar in the hydrogel with variable GAG content or the GAG sulfation and strongly depends on the molecular weight of the protein and the mesh size of the hydrogels. Moreover, while the GAG content of the hydrogel similarly regulated the diffusivity of heparin-affine proteins, selective removal of a particular sulfate group has a more protein-specific impact on the transport of heparin affine proteins.

### 2.3. VEGF165 Release from starPEG-GAG Hydrogels with Varied GAG Content and Sulfation Patterns

The effect of the heparin (derivative) concentration and sulfation pattern on the release of the VEGF165 from the respective

gels was evaluated for a duration of 360 h. Due to the use of a biorthogonal crosslinking reaction, the protein was directly loaded into the scaffolds during the hydrogel formation with the assumption of almost no covalent protein incorporation within the polymer networks.

The release of the VEGF165 from the GAG-free PEG hydrogel showed a significant initial burst (Figure 3A). More than 60% of the loaded protein was released within the first 24 h. At 72 h, the release of VEGF165 reached a maximal value with  $\approx 70\%$  of the initially loaded protein. By contrast, all heparin containing hydrogels retained more than 97% of the loaded VEGF throughout 360 h (Figure 3B), which could be attributed to the large molar excess of heparin over VEGF ( $\approx 400:1$ ) even for hydrogels with the lowest heparin concentration. The release of the VEGF165 can be gradually adjusted by varying the heparin concentration (Figure 3B), decreasing the heparin content of the hydrogel from  $1500 \times 10^{-6}$  to  $500 \times 10^{-6}$  M allowed to enhance the overall release of VEGF165 by a factor of three.

Hydrogels containing heparin derivatives with different sulfation patterns also displayed a variation in the release profile. Here, the sulfation degree of the heparin derivative was found to be inversely correlated to the amount of VEGF165 released from the hydrogel (Figure 3C). The cumulative release of VEGF165 within the first two weeks increased from  $\approx 1\%$  for Hep to  $\approx 2.5\%$  for 6O-DSH containing hydrogels. Moreover, incorporation of 6ON-DSH (with 33% sulfation degree) enhanced the VEGF release by  $\geq 4\%$  throughout 360 h. Interestingly, although 6ON-DSH contains only  $\approx 1/3$  of the sulfate groups of heparin, 96% of the proteins were retained within

this hydrogel even after two weeks, which is significantly higher than the amount remaining in the pure PEG hydrogel.

To understand if the release of the VEGF165 within the hydrogel is governed by both the diffusion of the protein through the hydrogel network and the binding to the GAG building block, the experimental release data was fit to the reaction–diffusion model in COMSOL Multiphysics. The curve fitting resulted in an estimate of the strength of the interaction between VEGF165 and the heparin or heparin derivatives within the crosslinked polymeric network. Our simulation results revealed that the reaction–diffusion model could describe the release profile of the proteins from all the hydrogel variants. The resulting binding affinity ( $K_A = 1/K_D$ ) of the VEGF165 to the heparin crosslinked within the hydrogel obtained from the curve fitting is inversely correlated to the sulfation degree of the GAG building blocks (Figure 3D). Besides, the  $K_D$  values obtained for the VEGF165–GAG interaction in the gel lie within the same order of magnitude as those obtained for the interaction of the protein with free heparin (derivatives) measured using microscale thermophoresis (MST), except for VEGF165 and 6ON-DSH, for which MST did not provide a binding curve/ $K_D$  value.

## 2.4. Local Availability of VEGF165 and Formation of Tubular HUVEC Networks in starPEG-GAG Hydrogels

VEGF is an important pro-regenerative growth factor that controls the proliferation, migration, survival, and differentiation of endothelial cells.<sup>[7a,12]</sup> Chwalek et al. demonstrated the potential of VEGF165 functionalized starPEG-GAG hydrogels to stimulate HUVECs to form a tubular network structure within three days.<sup>[1a]</sup> Since the administration of VEGF165 within the star-PEG-Hep gels may be crucial for the HUVEC sprouting, we investigated the role of the heparin (derivative) concentration and sulfation on the endothelial cell morphogenesis within hemispherical hydrogels (Figure 4A). HUVECs were cultured in soft hydrogels (storage moduli  $\approx 200$  Pa) containing matrix metalloproteinases (MMP)-cleavable peptides as crosslinkers to allow for the cell-mediated proteolytic matrix degradation.<sup>[5]</sup> The total loading of VEGF165 to the hydrogels was varied from 0 to 20  $\mu\text{g mL}^{-1}$  ( $(0\text{--}524) \times 10^{-9}$  M) to further modulate the free factor availability within the hydrogels. The concentration range was chosen since previous data showed that the functionalization of starPEG-GAG hydrogels containing a total heparin concentration of  $1500 \times 10^{-6}$  M with 5  $\mu\text{g mL}^{-1}$  ( $131 \times 10^{-9}$  M) of VEGF was necessary to initiate morphogenesis of embedded HUVECs.<sup>[1a]</sup>

First, to illustrate the effect of the free VEGF165 on HUVECs, we tested HUVEC growth on 2D with VEGF165 at concentrations between 0 and 100  $\text{ng mL}^{-1}$  ( $(0\text{--}2600) \times 10^{-12}$  M) and found a metabolic effect in a dose-dependent manner (Figure S6, Supporting Information). Similarly, others have also reported that VEGF concentrations between 10 and 20  $\text{ng mL}^{-1}$  ( $(260\text{--}520) \times 10^{-12}$  M) induced proliferation and the formation of tubular like structures of the HUVECs.<sup>[13]</sup>

Numerical simulations on the basis of the reaction–diffusion model,<sup>[10a,14]</sup> were carried out to determine the amount of the free factor presented to the cells right after gelation (0 h) and at

72 h after hydrogel gelation (i.e., after three days after culture) when the tubular endothelial structures are expected to form (Figure 4B). According to the simulation, the concentration of the free VEGF165 is inversely proportional to the GAG content of the hydrogel. At  $t = 0$  h, the pure PEG gel showed the highest concentration of free VEGF165 ( $\approx 130\,000 \times 10^{-12}$  M) whereas the corresponding concentrations within hydrogels containing a concentration of  $500 \times 10^{-6}$ ,  $1000 \times 10^{-6}$ , and  $1500 \times 10^{-6}$  M of heparin were found to be  $\approx 190 \times 10^{-12}$ ,  $110 \times 10^{-12}$ , and  $90 \times 10^{-12}$  M, respectively. After 72 h, a significant portion of the VEGF165 was already released from the pure PEG gel ( $\approx 6000 \times 10^{-12}$  M of VEGF165 in the medium) compared to the heparin-containing hydrogels ( $(\approx 40\text{--}80) \times 10^{-12}$  M of VEGF in the medium).

Similar trends were also observed for the hydrogels containing heparin derivatives with varying sulfation patterns (6ON-DSH, 6O-DSH, and Hep, corresponding to 33%, 67%, and 100% sulfation degree, respectively). After 72 h, the concentration of free VEGF165 within the hydrogel with the highest GAG sulfation (heparin) was  $\approx 90 \times 10^{-12}$  M. The concentration increased to  $\approx 260 \times 10^{-12}$  and  $\approx 390 \times 10^{-12}$  M for the hydrogel with 6O-DSH and 6ON-DSH, respectively. After 72 h, all hydrogels with varied GAG sulfation contained a similar amount of free factor as compared to 0 h with the amount of the free factor in the media inversely correlated to the sulfation degree of the heparin derivative.

Next, the impact of the heparin content and sulfation on the availability and activity of hydrogel entrapped VEGF165 was analyzed while the morphogenesis of HUVECs was examined. At any VEGF165 loading concentration (0, 1, 5, 20  $\mu\text{g mL}^{-1}$  ( $0 \times 10^{-9}$ ,  $26 \times 10^{-9}$ ,  $131 \times 10^{-9}$ ,  $524 \times 10^{-9}$  M)), the hydrogels containing the lowest heparin concentration ( $500 \times 10^{-6}$  M) displayed superior endothelial morphogenesis compared to any other hydrogels tested (Figure 4C). The total area of tubular structures and the number of branching points of the tubular HUVEC network structures were significantly higher in the hydrogel with the lowest heparin concentration than for hydrogels with the medium ( $1000 \times 10^{-6}$  M) or high ( $1500 \times 10^{-6}$  M) heparin concentration. In general, the extent of tubular morphogenesis decreased as the heparin concentration of the hydrogel increased. This effect was directly correlated with the amount of free VEGF165 within the hydrogel.

Furthermore, the amount of free VEGF165 in the gels enhanced the formation of tubular HUVEC networks in a concentration-dependent manner. In particular, in the hydrogel with the low ( $500 \times 10^{-6}$  M) and medium ( $1000 \times 10^{-6}$  M) heparin concentration, HUVEC morphogenesis increased as more VEGF165 was loaded into the hydrogel (Figure 4C). Notably, the hydrogel with the lowest heparin concentration also required a low VEGF165 loading to induce an extensive tubular network. Although 1  $\mu\text{g mL}^{-1}$  ( $26 \times 10^{-9}$  M) of VEGF165 was sufficient to induce HUVEC morphogenesis in the hydrogel with the low heparin concentration, increasing the VEGF165 loading up to 20  $\mu\text{g mL}^{-1}$  ( $524 \times 10^{-9}$  M) in both the hydrogels with the medium and a high GAG content could not promote a similar extent of HUVEC morphogenesis (Figure 4C). Interestingly, while the pure PEG hydrogel contained the highest amount of free VEGF165 within the system compared to the other types of hydrogels, a minimum level of tubular structures was observed within this hydrogel (Figure 4C). A slight increase in

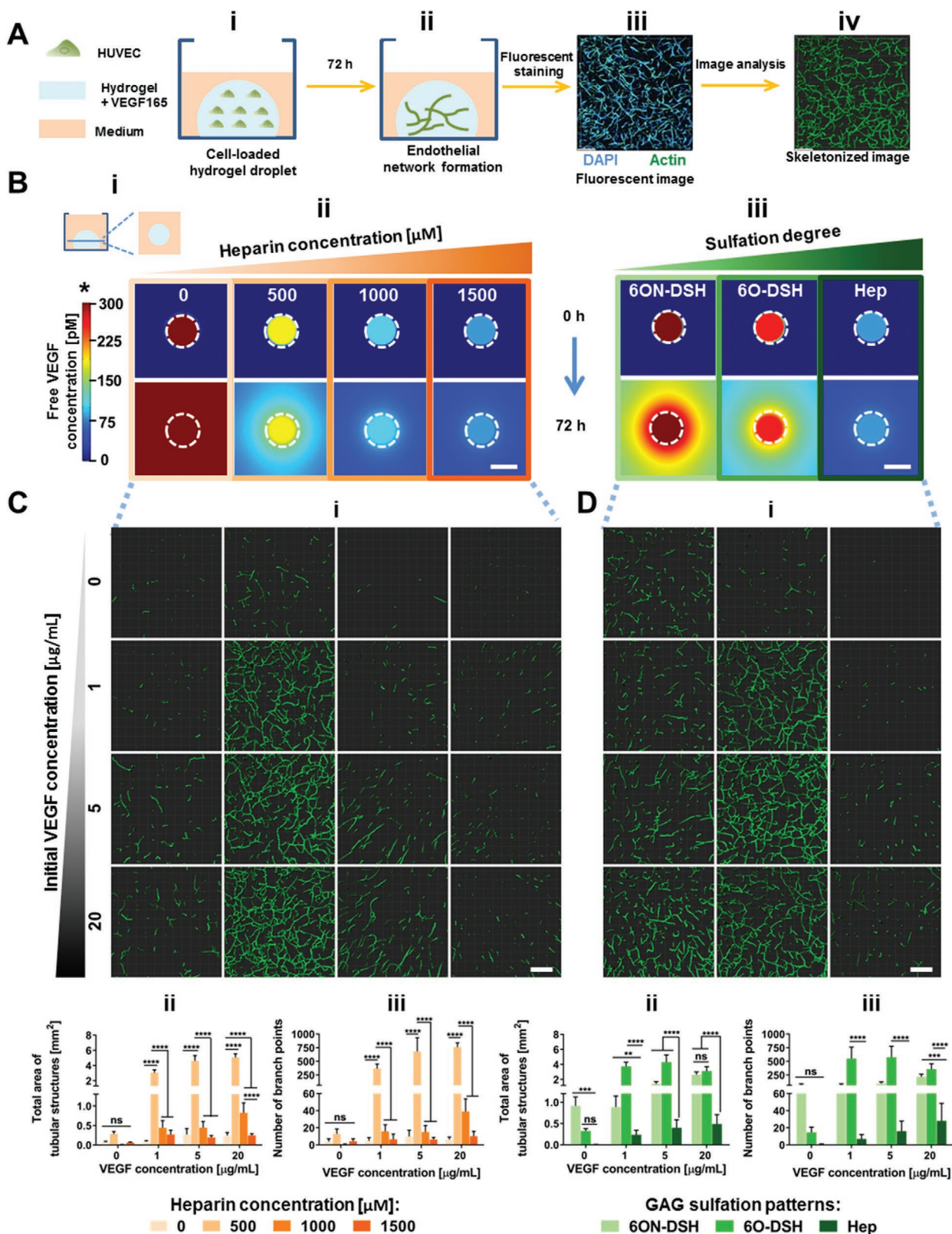


**Figure 4.** Local availability of free VEGF165 and GAG sulfation patterns control the formation of tubular HUVEC network structures within starPEG-GAG hydrogels. A) Scheme of the in vitro assay for studying the endothelial cell morphogenesis in cell-laden hydrogels. i) Uniform embedding of HUVECs and growth factors (VEGF165) within a hydrogel droplet. ii) The formation of capillary-like structures after three days of culture. iii) Fluorescence image of tubular HUVEC network structures within the hydrogel. DAPI was used as a nuclear counterstain, and the actin filament was visualized using

the formation of tubular HUVEC network structures was seen in the pure PEG gels when the VEGF165 loading was raised to 5 and 20  $\mu\text{g mL}^{-1}$ .

Similar to the effect of VEGF165 within the hydrogels with varying heparin concentration, HUVEC morphogenesis was enhanced in a concentration-dependent manner in the hydrogels with different GAG sulfation pattern (Figure 4D). Increasing the free factor concentration by removing the 6O or the 6O and the N sulfate groups (67% or 33% sulfation degree, respectively) from the heparin enhanced the formation of tubular HUVEC network structures. Compared to the hydrogel with the fully sulfated heparin (100% sulfation degree), the hydrogel containing 6O-DSH (67% sulfation degree) or 6ON-DSH (33% sulfation degree) produced HUVEC networks with a larger area of tubular structures and a higher number of branch points. Interestingly, at the lower VEGF165 loading concentrations of 1  $\mu\text{g mL}^{-1}$  ( $26 \times 10^{-9}$  M) and 5  $\mu\text{g mL}^{-1}$  ( $131 \times 10^{-9}$  M), a stronger formation of tubular HUVEC network structures was observed if hydrogels containing 6O-DSH (67% sulfation degree) were compared to the 6ON-DSH hydrogels with low (33%) sulfation degree despite the higher estimated free VEGF165 in the 6ON-DSH hydrogels. However, increasing the VEGF165 loading to 20  $\mu\text{g mL}^{-1}$  ( $524 \times 10^{-9}$  M) did not result in a significant difference in the HUVECs capillary network area for 6O and 6ON-DSH hydrogels (33% sulfation degree) (Figure 4D). Notably, in the absence of the VEGF165, the hydrogel containing the heparin derivative with the lowest sulfation promotes the formation of larger tubular structures areas compared to the ones with higher GAG sulfation (Figure 4D).

## 2.5. Tubular HUVEC Network Formation in starPEG-GAG Hydrogels with Spatially Graded Distribution of VEGF165

As discussed above, hydrogels containing  $500 \times 10^{-6}$  M of heparin that has been uniformly functionalized with the VEGF165 were shown to support the formation of dense and highly branched tubular HUVEC networks. In order to test the applicability of this hydrogel to direct the distribution of tubular HUVEC network structures, VEGF165 was presented as a gradient utilizing a microfluidic device (Figure 5A). Time-lapse fluorescence imaging revealed the formation of a VEGF165 gradient across the hydrogel channel over 72 h (Figure 5A).

Immediately after the addition of the growth factors to the microfluidic channel, a significant amount of the protein was accumulated near the medium-gel interface. The simulation of the spatial-temporal profile of the gradient of VEGF165 using the reaction-diffusion model indicated that the gradient only spans across the first 300  $\mu\text{m}$  of hydrogel from the source of the growth factors and remains stable for up to 72 h (Figure 5B). In good agreement with the results of the simulation, the fluorescent protein gradient mostly spread within the first half of the hydrogel channel from the source of the growth factors. The gradient was stable during the whole experiment (i.e., over 72 h), although no medium flow was applied to the medium nor the growth factor channel (Figure 5C).

To examine the effect of the VEGF165 gradient on the spatial formation of tubular structures, HUVECs were embedded within the hydrogel. To form a cell-instructive gradient, the left supply channel was subsequently filled with a VEGF165-containing solution (5  $\mu\text{g mL}^{-1}$  ( $131 \times 10^{-9}$  M)). The formation of tubular HUVEC network structures within the VEGF165 gradient was compared to the structure formation in hydrogels without VEGF165 and in hydrogels that have been homogeneously preloaded with VEGF165 (Figure 5D). After three days of culture, the extent of tubular structures (expresses as the total area of the tubular network) near the sink channel, the source channel, as well as at overall hydrogel channel volume was quantified (Figure 5E). The hydrogel without VEGF165 functionalization did not support the formation of any tubular structures. For the gels containing the VEGF165 gradient, we observed a higher density of tubular structures toward the higher growth factor concentration (Figure 5F). Moreover, when VEGF165 was homogeneously distributed within the hydrogel, the extent of the tube-like structure formation in the source and sink volume of the hydrogel channel was comparable.

VEGF gradients were also used to regulate endothelial sprout orientation during sprouting morphogenesis in biopolymer-derived matrices.<sup>[15]</sup> However, in our study, we did not observe any significant difference in the orientation of the emerging tubular structures at different locations within the hydrogel channel between the cell-laden hydrogels when conditioned with uniform or graded distributions of VEGF (data not shown). This result might be explained by differences in the cell-morphology assay set-up (e.g., differences in the initial cell distribution, orientation, and polarization compared to sprouting assays).

ATTO-633-phalloidin. iv) The skeletonized image obtained from the fluorescence image for the quantification of the number of branching as well as the total area of the capillary network. B) Surface plots generated in COMSOL Multiphysics for the plane indicated in i) of the free VEGF165 concentration in hydrogel droplets containing ii) varying amounts of heparin and iii) heparin derivatives with different degrees of sulfation. The gels were "preloaded" with 5  $\mu\text{g mL}^{-1}$  ( $131 \times 10^{-9}$  M) VEGF165. The colors show the distribution of the free VEGF165 within the media and the hydrogel just after the gel formation (0 h) and 72 h after incubation of the hydrogels with media. The free factor with a concentration of  $300 \times 10^{-12}$  M or higher is shown with the same color (dark red) as indicated by the \* sign. Scale bar = 4 mm. C) Effect of the heparin concentration on the HUVEC capillary morphogenesis at various initial concentrations of VEGF165 (0, 1, 5, 20  $\mu\text{g mL}^{-1}$  ( $0 \times 10^{-9}$ ,  $26 \times 10^{-9}$ ,  $131 \times 10^{-9}$ ,  $524 \times 10^{-9}$  M)). i) Representative skeletonized images of tubular HUVEC network structures formed within the hydrogels with heparin concentrations ranging from 0 to  $1500 \times 10^{-6}$  M over three days. ii) Total area of tubular HUVEC structures. iii) Number of branching points of the endothelial cell network. D) Effect of GAG sulfation on the endothelial capillary morphogenesis at various initial concentrations of VEGF165 (0, 1, 5, 20  $\mu\text{g mL}^{-1}$  ( $0 \times 10^{-9}$ ,  $26 \times 10^{-9}$ ,  $131 \times 10^{-9}$ ,  $524 \times 10^{-9}$  M)). i) Representative skeletonized images of HUVEC network structures formed within the hydrogels containing heparin derivatives with varied sulfation patterns (6ON-DSH, 6O-DSH, and Hep corresponding to 33%, 67%, and 100% sulfation degree, respectively) over three days. ii) Total area of the tubular HUVEC network structures. iii) Number of branching points of the endothelial cell network. Fixed samples were stained with phalloidin and DAPI, and Imaris software was used to process and skeletonize the fluorescence images. One image per condition was chosen arbitrarily to represent different hydrogel conditions. Scale bar = 200  $\mu\text{m}$ . Data represents mean  $\pm$  SD for  $n = 5-8$  cultures, "ns" stands for not significant, \*\* $P < 0.01$ , \*\*\* $P < 0.001$ , and \*\*\*\* $P < 0.0001$ .



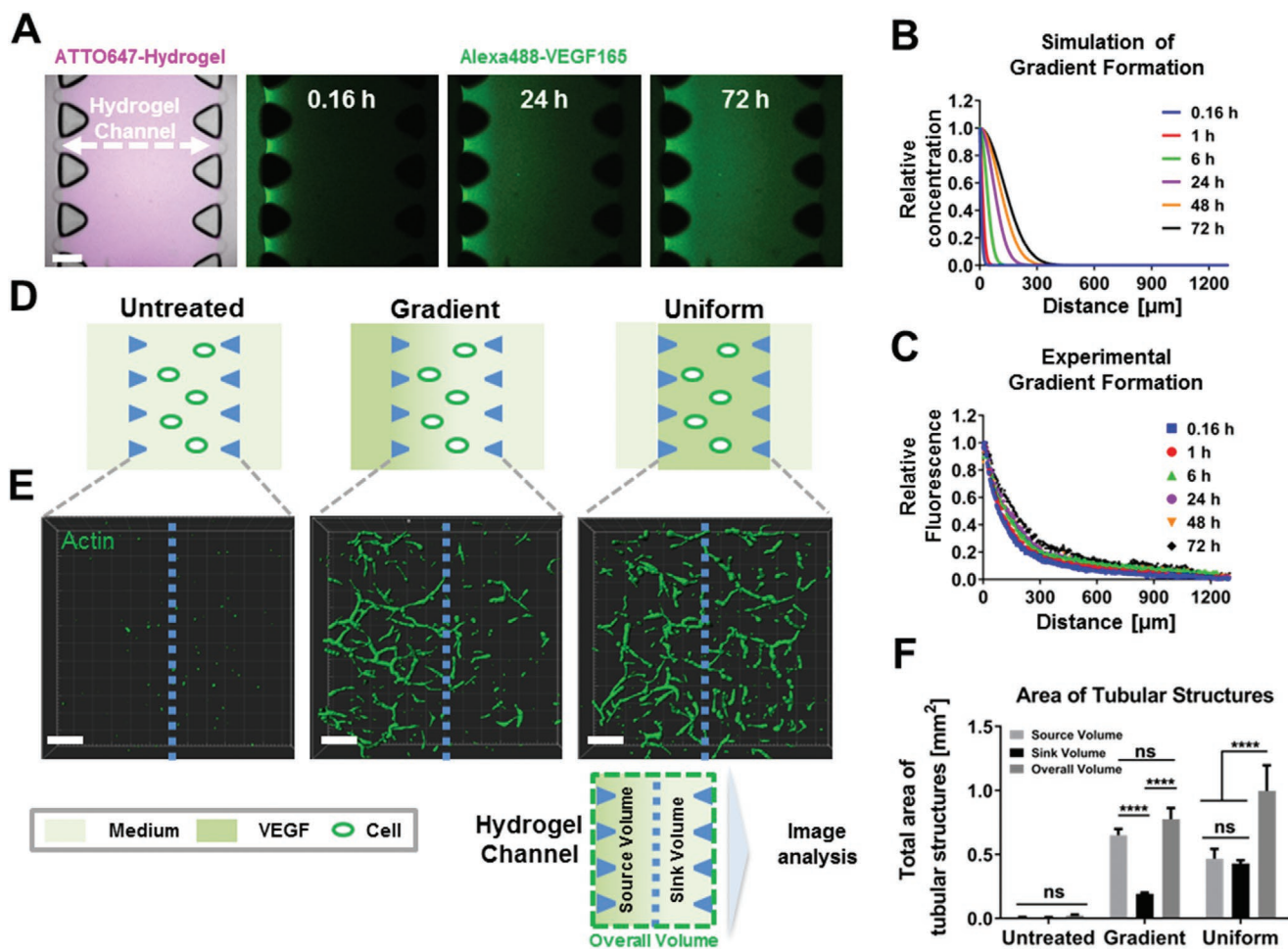


**Figure 5.** The distribution of VEGF165 modulates the formation and spatial organization of tubular HUVEC structures within starPEG-GAG hydrogels. VEGF165 gradient was formed in the starPEG-Hep hydrogel with a heparin concentration of  $500 \times 10^{-6}$  M. A) Fluorescence images representing the gradient of fluorescently labeled VEGF165 formed within the microfluidic channel after 72 h. B) Spatiotemporal distribution of VEGF165 calculated based on a reaction–diffusion model in COMSOL Multiphysics. C) Experimentally determined gradient of fluorescently labeled VEGF165 in the microfluidic channel. D) Set-up to investigate the effect of the VEGF165 gradient on the spatial formation of tubular structures. The endothelial cells were either cultured in hydrogels without supplement of VEGF165, under the action of a VEGF165 gradient within the hydrogel or in hydrogels that have been homogeneously preloaded with VEGF165. E) Representative skeletonized images of tubular HUVEC network structures resulting from the matrix-mediated presentation of VEGF165 under the conditions outlined in (D) after cultivation for three days. Fixed samples were stained with phalloidin and DAPI, and the Imaris software was used to process and skeletonize the fluorescence images. F) Quantification of the total area of the tubular structures at a different location within the hydrogel channel. The source volume is defined as the half volume of the hydrogel channel close to the source of the VEGF, whereas the sink volume is defined as the half volume of the hydrogel channel close to the channel containing no VEGF. The overall volume is the sum of the sink and source volume of the hydrogel channel. Scale bar = 200  $\mu$ m. Data represent mean  $\pm$  SD for  $n = 3$ , “ns” stands for not significant, \*\*\*\* $P < 0.0001$ .

### 3. Discussion and Conclusions

VEGF controls the initiation of vasculogenesis and angiogenesis.<sup>[7a,12]</sup> Therefore, the factor has been widely applied to control the vascularization of engineered biomaterials.<sup>[1a,16]</sup> Approaches to maintain the stability of the protein and its retention within polymeric biomaterials include covalent immobilization,<sup>[17]</sup> engineering factor variants with higher affinity for particular matrices,<sup>[18]</sup> and incorporation of GAGs into polymer networks to reversibly complex the factor.<sup>[1d,f]</sup> The latter approach offers particularly valuable options to enhance the bioactivity of VEGF since GAG-complexation can protect the protein against degradation and facilitate its binding to

cellular receptors.<sup>[1e,16b,19]</sup> Previously, the effective stiffness of starPEG-GAG hydrogels, supportive combination of proangiogenic growth factors, and the relevance of supporting cells have been identified to enable a versatile 3D in vitro model of angiogenesis.<sup>[1a]</sup> However, the impact of GAG sulfation pattern and GAG concentration of the hydrogel on the morphogenesis of gel-embedded vascular endothelial cells was not yet determined despite of the known importance of both parameters on availability and activity of VEGF165.<sup>[1d,20]</sup>

To systematically and quantitatively dissect the relevance of both parameters for growth factor-mediated cell fate control, we herein first prepared starPEG-GAG hydrogels of comparable mechanical properties but varying GAG concentration

and sulfation patterns and examined the impact of the different network parameters on the diffusivity of selected soluble signaling molecules, including VEGF165. Second, we analyzed the release of VEGF165 from starPEG-GAG hydrogels using a reaction–diffusion model as well as experimental release studies and revealed the interplay between the protein–GAG interaction within the polymer network and the resulting global transport phenomena. Third, supported by mathematical modeling, tubular HUVEC morphogenesis within starPEG-GAG hydrogels was studied in dependence on the respective VEGF165 availability. Finally, the distribution of VEGF165 within the hydrogels was graded by microfluidic methods to modulate the spatial organization of HUVEC tubular network formation.

The approach is based on the previously established rational polymer network design for decoupling of mechanical and biochemical properties of starPEG-GAG hydrogels,<sup>[21]</sup> which allowed for the targeted preparation of gels with a stiffness ranging from 0.2 to 8 kPa at invariant GAG concentration and of gels with similar mechanical properties and variable GAG sulfation patterns, respectively.<sup>[4–5]</sup> In here, the hydrogel system was extended to vary the GAG concentration over an even broader range ( $(500–1500) \times 10^{-6}$  M) at invariant soft mechanical properties (Figure 1E). Furthermore, we prepared hydrogels with components of different GAG sulfation patterns using selectively desulfated heparin derivatives as building blocks (Figure 1F).

Based on that, the impact of the GAG concentration and sulfation pattern on the diffusivity of selected signaling molecules of different dimensions and heparin-affinity was investigated (Figure 2). Our analysis revealed that the diffusivity of the nonaffine proteins was primarily controlled by their molecular weight and mesh size of hydrogel but not by the total GAG concentration of the hydrogel (Figure 2, and Figures S4 and S5, Supporting Information). In contrast, the diffusivity of the affine proteins was minimally affected by their molecular weight and decreased as the GAG content of the hydrogel increased, clearly pointing to the predominant role of sulfate group mediated electrostatic interactions with positively charged amino acid residues within the GAG affine signaling molecules (Figure 2A). This trend is similar to what Jha and co-workers reported for the diffusion of TGF $\beta$ 1 (another heparin-affine protein) in heparin-containing hyaluronic acid-based hydrogels.<sup>[22]</sup> The effect of the heparin concentration on the in-gel diffusion of the heparin-affine proteins, here demonstrated for VEGF165, was further correlated with the release from the hydrogel matrices (Figure 3B). We observed an increasing VEGF165 release from the hydrogels as the GAG content decreased, which is in line with previous reports on the retention and release rate of VEGF165 from other GAG-based hydrogel systems<sup>[16a,23]</sup> and proved again the importance of the sulfate group mediated interactions with signaling molecules that carry positively charged patches or binding sites.<sup>[8,24]</sup>

The affinity of soluble GAG-binding signaling molecules to GAGs in solution is mainly governed by the GAG-specific sulfation pattern, i.e., the sulfation degree and spacing along the polysaccharide's backbones.<sup>[25]</sup> Several protocols for the sulfation and desulfation of GAGs have been developed and applied to tune the binding of signaling molecules.<sup>[4,26]</sup> However, due to the spatial arrangement of the GAGs in a 3D polymer

network and the distribution of the GAGs within the hydrogel space, additional parameters that affect protein binding to the hydrogel may arise. Based on our previous work,<sup>[4]</sup> we herein studied the molecular transport of different growth factors in hydrogels containing heparin or heparin derivatives of varied sulfation patterns.

While the GAG concentration of the gels similarly governed the transport of a positively charged growth factor (VEGF165) and a positively charged chemokine (SDF1 $\alpha$ ), the specific GAG sulfation pattern was found to affect the in-gel diffusivity of some particular proteins only (Figure 2B). In line with previous findings,<sup>[20,27]</sup> some proteins were shown to preferentially interact with a distinct sulfate group of the heparin: While the removal of 6O-sulfate did not significantly affect the diffusivity of SDF1 $\alpha$  in starPEG-GAG gels, it significantly enhanced the effective diffusion coefficient of VEGF165 (N- and 6O-sulfate groups mediate the binding of VEGF165 to heparin, whereas the interaction with SDF1 $\alpha$  mainly involves the 2O- and N-sulfate groups).<sup>[20,27b,c]</sup> The diffusivity of VEGF165 within starPEG-GAG hydrogels displaying different GAG sulfation patterns does also correlate with the VEGF165 release from the gels (Figure 3C). Hydrogels containing 6O-DSH (67% sulfation degree) released significantly more VEGF165 than gels containing fully sulfated heparin (100% sulfation degree), the release further increased if the GAG building block of the hydrogel was changed from 6O-DSH to 6ON-DSH heparin (33% sulfation degree). This observation that inversely correlates the diffusivity of GAG affine proteins with the hydrogel sulfation degree is in good agreement with previously reported release data of VEGF165 from starPEG-GAG hydrogels containing desulfated heparin derivatives.<sup>[1d]</sup>

Mathematical models have been previously applied to predict the transport of growth factors within GAG-based materials in the presence or absence of matrix degradation.<sup>[14a,b,28]</sup> However, a direct comparison between the experimental and the theoretical release was not yet presented. Herein, a reaction–diffusion model was used to estimate the VEGF165 release from hydrogels made of differently sulfated GAGs and to derive the  $K_D$  values characterizing the stability of the gel-contained VEGF-GAG complexes. A decrease in the GAG sulfation resulted in a weaker interaction between the protein and the GAG within the hydrogels. The binding strength of VEGF165 to the GAG-component of the hydrogel estimated by the mathematical model was found to be comparable to the dissociation constant of soluble VEGF165-GAG complexes as experimentally determined by MST (Figure 3D). This creates a basis for the in silico prediction of the transport of different GAG-binding proteins within the hydrogels using the MST-derived  $K_D$  values.

The GAG volume density of the hydrogel governs the local availability of free factor within the hydrogel network and thereby controls the vascular morphogenesis of gel-embedded endothelial cells. We, therefore, applied the developed mathematical model to predict the available concentration of VEGF165 within the polymer network used in HUVEC tubulogenesis experiments. Despite the high retention of the VEGF165 ( $\geq 90\%$ ) in all starPEG-Hep hydrogels (Figure 3B), only the hydrogels with  $500 \times 10^{-6}$  M of heparin supported extensive HUVEC morphogenesis. This can be explained by elevated concentrations of the freely diffusible factor

in hydrogels of decreased GAG concentration (Figure 4B). Based on our simulation results for scaffolds with  $5 \mu\text{g mL}^{-1}$  ( $131 \times 10^{-9} \text{ M}$ ) VEGF165 loading, hydrogels containing  $500 \times 10^{-6} \text{ M}$  heparin can maintain free VEGF165 concentrations of about  $180 \times 10^{-12} \text{ M}$ , for at least three days of culture. This concentration is comparable to the VEGF dose reported to be required for HUVEC capillary network formation in other biopolymer-based matrices ( $\approx 520 \times 10^{-12} \text{ M}$ ).<sup>[13a,c]</sup> Out of our set of gels, however, only the material containing the lowest heparin concentration induced the formation of tubular HUVECs structures at any VEGF165 loading concentration (Figure 4C). Increasing the amount of VEGF165 loading to  $20 \mu\text{g mL}^{-1}$  ( $524 \times 10^{-9} \text{ M}$ ) to the hydrogels with high or medium heparin concentration of  $1000 \times 10^{-6}$  or  $1500 \times 10^{-6} \text{ M}$  did not enhance tubular morphogenesis as much as in the hydrogel with the lowest heparin concentration despite of the elevated concentrations of free VEGF165. However, since heparin is known to bind a plethora of growth factors,<sup>[1e]</sup> the availability of endogenously secreted factors (not analytically determined for our system) can be reasonably assumed to be similarly influenced by the GAG concentration and sulfation pattern.

Furthermore, the impact of the available amounts of VEGF165 on HUVEC morphogenesis obviously depends on the specific GAG sulfation pattern of the gel building blocks (Figure 4C). According to the simulations, a complete removal of the heparin component (i.e., a pure PEG gel) or the substitution of fully sulfated heparin with the 6O- or 6ON-desulfated derivative strongly increases the availability of free VEGF165 (Figure 4B). However, HUVEC tubulogenesis significantly enhanced only in the starPEG-6O-DSH hydrogel but not in the starPEG-6ON-DSH or pure PEG hydrogels. This can be attributed to the fact that heparin has been recognized to prolong the half-life of the heparin-binding proteins in culture by increasing their stability.<sup>[19b,29]</sup> Moreover, as previously demonstrated for the heparin-binding factor BMP-2, N-DSH, and 6ON-DSH are not as effective as the native heparin in preserving the bioactivity of BMP-2.<sup>[30]</sup> Therefore, we hypothesize that the presence of the heparin and, more specifically, the N-sulfate group of heparin is essential to maintain the activity of VEGF165. The capacity of starPEG-heparin hydrogels to enhance the activity of VEGF165 could also explain the relatively low concentration of free VEGF165 needed to stimulate the formation of tubular structures within these hydrogels. In particular, the hydrogel with the lowest heparin concentration ( $500 \times 10^{-6} \text{ M}$ ) could stimulate the endothelial morphogenesis at a free VEGF165 concentration of  $\approx 40 \times 10^{-12} \text{ M}$  (for  $1 \mu\text{g mL}^{-1}$  of total VEGF165 loading, data not shown) whereas in hydrogel systems without heparin significantly higher VEGF concentrations ( $\geq 1300 \times 10^{-12} \text{ M}$ ) were required to induce the formation of tubular HUVEC structures.<sup>[31]</sup>

Finally, we locally controlled the administration of VEGF165 within the hydrogel using a microfluidic platform to direct the formation of capillary-forming HUVEC structures. The hydrogel matrix with the lowest GAG concentration was chosen as it was superior in supporting tubular HUVEC morphogenesis. Previous studies applied photocrosslinking to locally support or inhibit cell-mediated polymer network degradation,<sup>[32]</sup> or RGD ligand presentation to locally activate HUVEC morphogenesis within hydrogels.<sup>[33]</sup> In our study,

numerical simulations based on the reaction diffusion-model enabled the prediction of the spatial and temporal distribution of VEGF165 within the microfluidically loaded starPEG-GAG hydrogels (Figure 5A–C). The spatially varying VEGF165 concentrations were shown to control the local formation of HUVEC capillary network structures within the GAG-based hydrogel matrices (Figure 5D–F). Compared to photopatterning techniques, our approach allows for utilizing different isoforms of VEGF, which act complementarily.<sup>[34]</sup> Microfluidic approaches have been applied before to generate graded distributions of signaling molecules within biomaterials aiming at spatiotemporal cell fate patterning.<sup>[35]</sup> However, the absence of growth factor-affine moieties (e.g., GAG units) within the used material may require a continuous flow of rather high amounts of growth factors from feeding solutions. This does not only produce significant constraints for the tunability and elevated costs, but it may also interfere with the paracrine signaling in the stimulated cultures in undesired ways. In contrast, our approach of applying GAG-based hydrogel matrices allowed for generating stable growth factor gradients for up to 72 h without growth factor perfusion. Moreover, the above-described modulation of the hydrogel transport properties for VEGF165 provides additional options to control the gradient profile of the factor.

In sum, computational modeling can unravel materials parameters that effectively control cellular morphogenesis through the localized administration of soluble signaling molecules. In the elaborated example, tailoring the GAG concentration and sulfation pattern of biohybrid hydrogels is shown to direct the formation of tubular HUVEC network structures by modulating the local availability of VEGF165. Such theory-driven design of cell-instructive materials will pave the way for future precision tissue engineering.

## 4. Experimental Section

**Protein Labeling:** Recombinant human VEGF165 (referred to as VEGF here), VEGF121, EGF (Peprotech, USA), SDF1 $\alpha$  (Miltenyi Biotec, Germany), Thrombin from bovine plasma (Sigma-Aldrich, Germany) (Table S1, Supporting Information) were labeled with Alexa 488 NHS esters (N-hydroxysuccinimide esters) (Thermo Fisher Scientific, Germany) for 1 h at room temperature. Afterward, the proteins were purified twice from the unreacted dyes using Zeba Desalting columns with MWCO of 7 kDa (Thermo Fisher Scientific, Germany) following the manufacturer's instructions. The final concentration of the protein and the conjugated dyes were measured using a NanoDrop 1000 Spectrophotometer (Thermo Fisher Scientific, Germany). The final labeling degree was determined to be 1–2 labels per protein.

**Preparation of starPEG-GAG Hydrogels:** The components for the formation of the hydrogels, including maleimide-functionalized heparin (Hep), and heparin derivatives (6O- and 6ON-desulfated heparin (6O-DSH and 6ON-DSH,  $M_w \approx 15\,000$ ) were in house synthesized, and the hydrogels were prepared as previously described with slight modifications.<sup>[5]</sup> Briefly, thiol functionalized 4-arm starPEG (starPEG-SH) ( $M_w 10\,000$ , Polymer Source, Inc., Dorval, Canada) and maleimide functionalized heparin/heparin derivatives were dissolved in PBS at the appropriate molar ratio. To generate hydrogels with a variable sulfation pattern, solutions containing heparin ( $3 \times 10^{-3} \text{ M}$ ) or desulfated heparin derivatives were mixed with the starPEG-SH solution ( $\approx 1.8 \times 10^{-3} \text{ M}$ ). Furthermore, heparin solution ( $1 \times 10^{-3}$  and  $2 \times 10^{-3} \text{ M}$ ) was mixed with starPEG-SH ( $1.5 \times 10^{-3} \text{ M}$ ) to produce hydrogels with a lowered heparin concentration ( $500 \times 10^{-6}$  and  $1000 \times 10^{-6} \text{ M}$ ). As a nonaffine hydrogel control, pure PEG hydrogels were prepared by reacting an equal volume

of starPEG-SH ( $3 \times 10^{-3}$  M) with maleimide-functionalized starPEG (starPEG-Mal) (JenKem Technology, Plano, USA). In general, upon the mixing of gel components, the hydrogels were formed instantaneously within several seconds. The pH of the starPEG-SH solution was adjusted to 5.6 to have an efficient hydrogel component mixing allowing the formation of homogenous hydrogel samples.

The synthesis of matrix metalloproteinase—cleavable peptide (MMP) with a sequence of Ac-CGGPQG-IWGQGCG and its conjugation with four arms polyethylene glycol (starPEG,  $M_w = 16\,500$  g mol $^{-1}$ ) was performed as previously described.<sup>[5]</sup> The starPEG-MMP conjugate was used in all the cellular experiments in place of noncleavable starPEG-SH.

**Rheological and Volume Swelling Measurements:** The hydrogel mixture (67  $\mu$ L) was allowed to polymerize between two hydrophobic coverslips with a diameter of 9 mm to produce free-standing hydrogel discs. After the polymerization, the coverslips were removed, and the hydrogels were scanned using an FLA 5100 fluorescence scanner (Fujifilm, Tokyo, Japan) before and after overnight swelling in PBS with excitation at 473 nm and an emission filter of 510 nm. The diameter of the hydrogel was then determined by analyzing the fluorescence images using the Fiji (ImageJ, NIH). The gel volumetric swelling,  $Q$  was determined by the following equation

$$Q = \left(\frac{d}{d_0}\right)^3 \quad (1)$$

where  $d_0$  and  $d$  are the initial and final diameter of the gel disk, respectively. Subsequently, the storage modulus of the swollen hydrogel was measured using rotational rheometry with 25 mm parallel plate geometry in an Ares LN2 (TA Instruments, Germany), as previously described.<sup>[5]</sup> The frequency sweeps were carried out at a shear frequency range from  $10^{-1}$  to 100 rad s $^{-1}$  with a strain amplitude of 2%. The mean values of the storage modulus were calculated from at least three independent hydrogel samples.

The mesh size of the hydrogels was calculated using the rubber elasticity theory, assuming an affine polymer network model from the storage moduli considering a fully elastic recovery of the hydrogel upon a relatively small deformation within the rheometric measurements (<20%).<sup>[9]</sup> Based on that, the theoretical hydrogel mesh size,  $\xi$  is estimated using the following equation

$$\xi = \left(\frac{G' N_A}{RT}\right)^{\frac{1}{3}} \quad (2)$$

where  $G'$  is the storage modulus,  $N_A$  is the Avogadro constant,  $R$  is the molar gas constant, and  $T$  is the measurement temperature.

**Determination of Protein Binding Affinity to GAG and GAG Derivatives:** MST was used to quantify the strength of interactions between the proteins and heparin or heparin derivatives, as previously described.<sup>[36]</sup> First, the proteins were labeled with a reactive fluorescence dye, NT-647, using the Monolith NT Protein labeling kit Red-NHS according to the manufacturer's (NanoTemper Technologies) instructions. The protein was purified from the unreacted dye using gel filtration columns (Sephadex G25, GE Healthcare) and the protein concentration and the purity was monitored using NanoDrop 1000 Spectrophotometer (Thermo Fisher Scientific, Germany) by measuring the absorption at 280 nm, and 650 nm for proteins and the dye, respectively.

For the thermophoresis experiment, heparin or heparin derivatives (titrated from  $15.25 \times 10^{-9}$  to  $1000 \times 10^{-6}$  in PBS containing Tween 20 (0.05%) and of bovine serum albumin (BSA) (0.1%)) were mixed with labeled proteins ( $(4-8) \times 10^{-9}$  M) in a 1:1 volume ratio. The mixture was then briefly centrifuged for 5 min at  $5000 \times g$  and 4 °C. Next, the sample mixture was loaded into hydrophobic capillaries (NanoTemper Technologies), and the thermophoresis measurement was carried out at 22 °C in the Monolith NT.115Pico instrument (NanoTemper Technologies) using excitation and MST power of 20% and 40%, respectively. Four independent measurements were carried out for each

heparin–protein pair, and the data were pooled and analyzed using the MO. Affinity Analysis software v2.2.4 (NanoTemper Technologies).

**Protein Release Studies from Hydrogels:** Hydrogel precursor solution (10  $\mu$ L) were mixed with proteins (500 ng) and allowed to polymerize as a gel droplet on a hydrophobic 8 wells  $\mu$ -slide (Ibidi, Germany). The release medium (400  $\mu$ L) containing endothelial cell growth medium (ECGM; Promocell, Heidelberg, Germany) supplemented with BSA (0.1%), and procline (0.1%) was added onto the hydrogel samples and incubated at 37 °C to allow the release of protein into the medium. The release medium was completely removed and exchanged with an equal volume of the fresh medium after 1, 6, 24, 72, 120, 168, 264, and 360 h. The collected media were then stored and frozen at  $-80$  °C until the analysis. The amount of protein in the release media was quantified for every time point using enzyme-linked immunosorbent assay (ELISA) DuoSet kit (R&D Systems, Minneapolis, USA) according to manufacturer's instructions ( $n \geq 6$ ).

**Fluorescent Recovery after Photobleaching:** FRAP was used to evaluate the mobility of proteins within the hydrogels or buffer. For the sample preparation, the hydrogel precursors were dissolved in PBS containing BSA (0.1%). Hydrogels were loaded with fluorescently-labeled proteins (a final concentration of  $2.5 \mu$ mol L $^{-1}$ ) during the gelation process. Moreover, to ensure that the diffusion coefficient measurement was carried out within the gel matrix and to specify the location of the bleached spot within the scaffold, the hydrogels were also spiked with ATTO 647 maleimide (1 mol%) (Atto-Tec, Siegen, Germany). For the FRAP measurement, the hydrogel mixture (3  $\mu$ L) were spread onto a glass slide to generate hydrogel with  $\approx 120 \mu$ m thickness, covered with the buffer solution (10  $\mu$ L) containing the same concentration of proteins as in the hydrogel, and sandwiched with another cover glass separated by an imaging spacer (Grace Bio-Labs SecureSeal, Sigma-Aldrich). Afterward, FRAP was carried out with a Leica TCS SP5 confocal using a 10 $\times$  magnification objective (HC PL Fluotar 0.30 NA). For each measurement, a time-series of 20 prebleach images with a resolution of  $256 \times 256$  pixels was recorded using an attenuated argon laser beam (80% output and 4% of transmission) every 141 ms. After that, a uniform disk with a radius of 20  $\mu$ m in the middle of the hydrogel samples was bleached with a high intensity of 488, 576, and 495 nm lines of an argon laser at 100% transmission for  $\approx 600$  ms.

Immediately after the photobleaching, a stack of 100 images was acquired at low laser intensity (4% of transmission) for every 141 ms followed by the acquisition of 120 images at 1 s intervals to measure the extent of fluorescent recovery within the bleached spot. The temperature was kept constant at 30 °C during all experiments. The diffusion coefficients ( $D$ ) were extracted from the fluorescent recovery curve, as described elsewhere.<sup>[4,37]</sup> Briefly, the mean fluorescent intensities in the bleached spot were normalized according to Equation (3) to correct for the possible bleaching during the image acquisition

$$f(t) = \frac{I_{\text{ref}}(\text{pre})}{I_{\text{ref}}(t)} \cdot \frac{I_{\text{frap}}(t)}{I_{\text{frap}}(\text{pre})} \quad (3)$$

where  $f(t)$  is the normalized fluorescent intensity in the bleached spot,  $I_{\text{frap}}(t)$  and  $I_{\text{ref}}(t)$  represent fluorescent intensities in the bleached spot and the reference region for every time point  $t$ , respectively, and the  $I_{\text{ref}}(\text{pre})$  and  $I_{\text{frap}}(\text{pre})$  represent fluorescent intensities in the reference region and the specified bleached spot before the bleaching, respectively.

Subsequently,  $f(t)$  was normalized to a full scale,  $F(t)$  using Equation (4). Here,  $f(0)$  is the normalized fluorescent intensity of the bleached spot just after the bleaching and  $f(\text{pre})$  is the normalized fluorescent intensity before the bleaching

$$F(t) = \frac{f(t) - f(0)}{f(\text{pre}) - f(0)} \quad (4)$$

Characteristics diffusion time  $\tau_D$  and the mobile fraction were then extracted from the least square fit of  $F(t)$  to the Equation (5) which is

based on 2D diffusion model for a circular spot as described previously by Soumpasis<sup>[38]</sup>

$$F(t) = a \cdot e^{-\frac{\tau_D}{2t}} \left[ I_0\left(\frac{\tau_D}{2t}\right) + I_1\left(\frac{\tau_D}{2t}\right) \right] \quad (5)$$

where  $I_0$  and  $I_1$  represent modified Bessel functions of the first kind of zero and first order, consecutively. Finally, the diffusion coefficient,  $D$ , was obtained from Equation (6), where  $w$  is the radius of the bleached area

$$D = \frac{w^2}{\tau_D} \quad (6)$$

**Characterization of the VEGF165 Gradient:** Commercially available microfluidic chips (AIM BIOTEC, Singapore), as described in detail elsewhere,<sup>[39]</sup> were used to generate a biomolecular gradient within the hydrogels. The microfluidic device consists of three parallel channels, including the growth factor, hydrogel, and medium channels with a wide of 0.5, 1.3, and 0.5 mm, respectively (Figure S7A, Supporting Information). The growth factor and the medium channel are separated from the hydrogel channel by trapezoid pillars with 0.1 mm spacing between the structures.

To characterize the protein gradients, the protein was labeled with Alexa-488 (please see the protein labeling procedures section), while the hydrogel was spiked with ATTO-647 (0.1%). Moreover, for all the growth factor gradient related experiments, including cellular experiments involving these microfluidic devices, the hydrogel precursors (10  $\mu$ L) were mixed thoroughly and subsequently injected into hydrogels. The gels were allowed to polymerize for 5 min, and the gel inlets were then sealed with adhesive sealant.

To initiate the gradient formation, a volume of fluorescently labeled protein (120  $\mu$ L of  $1 \times 10^{-6}$  M) diluted with PBS/BSA (0.1%) solution was injected into the growth factor channels, whereas the same volume of PBS/BSA (0.1%) solution was loaded into the medium channel (Figure S7B, Supporting Information). For the time-lapse imaging, mineral oil (20  $\mu$ L) (Sigma-Aldrich, Germany) was added on to each medium and growth factor port to prevent evaporation during the imaging process. The fluorescence images were captured using a Leica TCS SP5 confocal (Leica Microsystems, Germany) every 30 min for a total duration of 48 h. Finally, a line profile was drawn using Leica application software along the width of the hydrogel image (LAS Software, Leica Microsystems, Germany), and subsequently, the fluorescence intensity was exported to analyze the spatial and temporal evolution of the protein gradient.

**Mathematical Model:** A reaction diffusion-model was used to predict the VEGF165 transport within the GAG-based hydrogels. Notably, the model was applied to analyze the protein release from a droplet of hydrogels and to determine the fraction of free/bound protein within a hydrogel droplet, as well as to estimate the spatial and temporal changes of the protein gradients within the microfluidic device. All the parameters required to generate each figure of the simulations are summarized in Table S3 (Supporting Information). Besides, the assumptions and the equations relevant for the computational modeling, as well as the experimental parameters such as the geometry and dimension of the hydrogel, volume of the buffer, etc. for each type of simulations, are described in detail in Section S1 (Supporting Information).

**Cell Cultures:** HUVECs were isolated as previously described,<sup>[40]</sup> and cultured in ECGM (Promocell, Heidelberg, Germany) containing supplemental and fetal calf serum (FCS) (2%) (SupplementMix C-39215, Promocell) on fibronectin-coated 75 cm<sup>2</sup> culture flasks, maintained at 5% CO<sub>2</sub> and 37 °C in a humidified incubator. After reaching 80% confluency, the cells were detached using trypsin-ethylenediaminetetraacetic acid (EDTA) (0.5%) (Sigma-Aldrich, München, Germany) solution, collected, centrifuged at 1000 rpm, and reseeded at appropriate density until further usage. Cells from passage 2–6 were used for all experiments.

**Endothelial Cell Vascular Morphogenesis:** To investigate the effect of GAG content on the endothelial morphogenesis within the hydrogel system, HUVECs were embedded within the hydrogels (a final heparin

concentration of  $0 \times 10^{-6}$ ,  $500 \times 10^{-6}$ ,  $1000 \times 10^{-6}$ , and  $1500 \times 10^{-6}$  M). Besides, the hydrogel with a varied GAG sulfation pattern (Hep, 6O-DSH, 6ON-DSH) (a total heparin concentration of  $1500 \times 10^{-6}$  M) was prepared to study the influence of the GAG sulfation pattern on the endothelial capillary morphogenesis. For these purposes, HUVECs were detached using Accutase (Sigma-Aldrich) for 5 min at 37 °C and resuspended in ECGM medium with supplemental mix and FCS (2%) at a final concentration of  $40 \times 10^6$  cells mL<sup>-1</sup>. Next, the starPEG-GAG hydrogels were prepared as described previously with slight modifications.<sup>[1a]</sup>

In brief, degradable starPEG-MMP conjugates ( $M_w$  16 500) and a heparin/heparin derivative-maleimide conjugates ( $M_w$  15 000) were separately dissolved in HUVEC culture medium. Subsequently, the adhesive peptide CWGGRGDSP (cRGD,  $M_w$  990) was supplemented into the heparin solution at a 2:1 molar ratio. After that, the heparin-RGD mixture was (nonreactively) functionalized with VEGF165 (PeproTech, USA) (a final concentration of 0–20  $\mu$ g mL<sup>-1</sup> ( $(0-524) \times 10^{-9}$  M)) and an equal volume of HUVEC suspension was added to generate a cell-heparin conjugate mixture. For the formation of hydrogels, the cell-heparin conjugate mixture was added to the starPEG conjugate solution in a 1:1 volume ratio to form hydrogel droplets (20  $\mu$ L), which were cast onto hydrophobic  $\mu$ -slides 8 well chambers (Ibidi, Germany). Following the in situ crosslinking, the gels were immediately immersed in the cell culture medium, and on day 3, the samples were fixed with 2% paraformaldehyde (PFA) for 10 min at RT and stained with the fluorescence.

For the spatial patterning of endothelial morphogenesis in microfluidic chip studies, hydrogels, and the growth factor were loaded into a commercially available microfluidic chip (AIM BIOTEC, Singapore). The final cell concentration within the hydrogel was  $10 \times 10^6$  cells mL<sup>-1</sup>. Afterward, the cells within the device were treated with VEGF165 (5  $\mu$ g mL<sup>-1</sup> ( $131 \times 10^{-9}$  M)) dissolved in medium either as a gradient or uniformly loaded within the hydrogels. The cells treated with the basal medium was also included as a control. The progress of the vascular morphogenesis was monitored every 24 h. On day 3, the cells were fixed with PFA (2%) and stained with phalloidin for the quantification of the total area of tubular structures formed in the half portion of the hydrogel channel close to the growth factor channel (source volume) and the medium channel (sink volume), as well as in the total volume of hydrogel channel (overall volume).

**Fluorescence Staining and Immunocytochemistry:** To analyze the extent of tubular structure formation in a hydrogel droplet or hydrogel embedded within the microfluidic channel, the cells were labeled according to the following protocol. After fixation and washing with PBS, the samples were permeabilized using Triton X-100 (0.1%) for 10 min. Samples were washed and incubated with Hoechst 33342 (Life Technologies; 1:200) and ATTO 610-phalloidin (Atto-Tec, 1:200) for two days at 4 °C. Next, the samples were washed three times and stored in PBS at 4 °C, covered with foil until the imaging using a Dragonfly Spinning Disc confocal microscope (Andor Technology Ltd., Belfast, UK). 10 $\times$  air objective was used to capture the image at a resolution of 1024  $\times$  1024 pixels and a pinhole of 20. For each hydrogel sample, a 200–300  $\mu$ m thick stack of images with a spatial resolution of 5  $\mu$ m (in the z-direction) was acquired.

**Image Analysis:** All the fluorescent images obtained from the Leica TCS SP5 and DragonFly Spinning Disc confocal microscopes were analyzed and processed using Leica application (LAS software, Leica Microsystems, Germany) or Imaris (Version 9.2.1, Bitplane AG, Zurich, Switzerland) software. The tiff images were exported and further processed with the Fiji (ImageJ, NIH) for a final visualization. To quantify the extent of tubular structure formation in 3D, 100  $\mu$ m thick z-stacks at 50  $\mu$ m above the glass slide were analyzed with Imaris (Version 9.2.1, Bitplane AG, Zurich, Switzerland) utilizing filament tracer module. Briefly, a threshold loops algorithm was used to generate a 3D skeletonized image of the tubular structures obtained from the phalloidin staining. All the parameters used for the fluorescent image segmentation are listed in Table S4 (Supporting Information). Next, the resulting skeletonized images were used to calculate the total area of tubular structures and the number of branch points, which represent the overall vasculature growth in the hydrogel and the complexity of the

structures, respectively. The skeletonized images were then visualized as a cone with a scale of 0.5.

**Statistical Analysis:** All experiments were repeated 2–3 times with at least three independent replicates. Statistical analysis and graphing were performed using the GraphPad Prism 6 (San Diego, California). A one-way analysis of variance (ANOVA) followed by Tukey's multiple comparison post hoc test was used to determine the level of significance between the groups with different treatments. All values represent the mean  $\pm$  standard deviation for at least three independent samples. The difference between the means was considered to be statistically significant at the level of  $P < 0.05$ .

## Supporting Information

Supporting Information is available from the Wiley Online Library or from the author.

## Acknowledgements

This work was supported by the Deutsche Forschungsgemeinschaft through ZI 1238/4-1 (Y.D.P.L. and R.Z.), CRC TR 67 (P.A., C.W., and U.F.), and FR 3367/2-1 (U.F.). Furthermore, the authors would like to thank Dr. Lars D. Renner (MBC Dresden) for the introduction with the FRAP experiments and Ning-Hui Lu for assistance with the release experiments.

## Conflict of Interest

The authors declare no conflict of interest.

## Author Contributions

Y.D.P.L. designed the study, performed experiments, developed mathematical models, analyzed data, and wrote the manuscript. P.A. discussed data and edited the manuscript. U.F. advised the study, discussed data, and edited the manuscript. C.W. supervised the study, discussed data, and edited the manuscript. R.Z. developed mathematical models, advised the study, discussed data, and edited the manuscript.

## Keywords

angiogenesis, diffusion, glycosaminoglycans, hydrogels, VEGF

Received: January 3, 2020

Revised: February 19, 2020

Published online: May 10, 2020

- [1] a) K. Chwalek, M. V. Tsurkan, U. Freudenberg, C. Werner, *Sci. Rep.* **2015**, *4*, 4414; b) M. O. Dellacherie, B. R. Seo, D. J. Mooney, *Nat. Rev. Mater.* **2019**, *4*, 379; c) U. Freudenberg, A. Hermann, P. B. Welzel, K. Stirl, S. C. Schwarz, M. Grimmer, A. Zieris, W. Panyanuwat, S. Zschoche, D. Meinhold, A. Storch, C. Werner, *Biomaterials* **2009**, *30*, 5049; d) U. Freudenberg, A. Zieris, K. Chwalek, M. V. Tsurkan, M. F. Maitz, P. Atallah, K. R. Levental, S. A. Eming, C. Werner, *J. Controlled Release* **2015**, *220*, 79; e) N. Lohmann, L. Schirmer, P. Atallah, E. Wandel, R. A. Ferrer, C. Werner, J. C. Simon, S. Franz, U. Freudenberg, *Sci. Transl. Med.* **2017**, *9*, eaai9044;

- f) A. Zieris, S. Prokoph, K. R. Levental, P. B. Welzel, M. Grimmer, U. Freudenberg, C. Werner, *Biomaterials* **2010**, *31*, 7985.
- [2] a) L. M. Caballero Aguilar, S. M. Silva, S. E. Moulton, *J. Controlled Release* **2019**, *306*, 40; b) J. Li, D. J. Mooney, *Nat. Rev. Mater.* **2016**, *1*, 16071; c) M. M. Martino, S. Brkic, E. Bovo, M. Burger, D. J. Schaefer, T. Wolff, L. Gürke, P. S. Briquez, H. M. Larsson, R. Gianni-Barrera, J. A. Hubbell, A. Banfi, *Front. Bioeng. Biotechnol.* **2015**, *3*, 45.
- [3] a) D. Gvaramia, E. Muller, K. Muller, P. Atallah, M. Tsurkan, U. Freudenberg, M. Bornhauser, C. Werner, *Biomaterials* **2017**, *138*, 108; b) H. M. Weber, M. V. Tsurkan, V. Magno, U. Freudenberg, C. Werner, *Acta Biomater.* **2017**, *57*, 59.
- [4] P. Atallah, L. Schirmer, M. Tsurkan, Y. D. Putra Limasale, R. Zimmermann, C. Werner, U. Freudenberg, *Biomaterials* **2018**, *181*, 227.
- [5] M. V. Tsurkan, K. Chwalek, S. Prokoph, A. Zieris, K. R. Levental, U. Freudenberg, C. Werner, *Adv. Mater.* **2013**, *25*, 2606.
- [6] P. Atallah, Y. D. P. Limasale, U. Freudenberg, C. Werner, *Faraday Discuss.* **2019**, *219*, 244.
- [7] a) R. S. Apte, D. S. Chen, N. Ferrara, *Cell* **2019**, *176*, 1248; b) J. Pauty, R. Usuba, I. G. Cheng, L. Hespel, H. Takahashi, K. Kato, M. Kobayashi, H. Nakajima, E. Lee, F. Yger, F. Soncin, Y. T. Matsunaga, *EBioMedicine* **2018**, *27*, 225.
- [8] a) H. G. Garg, R. J. Linhardt, C. A. Hales, *Chemistry and Biology of Heparin and Heparan Sulfate*, Elsevier, Oxford, UK **2011**; b) I. Capila, R. J. Linhardt, *Angew. Chem., Int. Ed.* **2002**, *41*, 390.
- [9] M. Rubinstein, R. H. Colby, *Polymer Physics*, OUP Academic, Oxford, N. Y. **2003**.
- [10] a) J. Crank, *The Mathematics of Diffusion*, Oxford University Press, Oxford, N. Y. **1975**; b) J. Witten, K. Ribbeck, *Nanoscale* **2017**, *9*, 8080.
- [11] a) S. T. Olson, H. R. Halvorson, I. Bjork, *J. Biol. Chem.* **1991**, *266*, 6342; b) S. T. Olson, Y. J. Chuang, *Trends Cardiovasc. Med.* **2002**, *12*, 331; c) W. J. Carter, E. Cama, J. A. Huntington, *J. Biol. Chem.* **2005**, *280*, 2745; d) P. D. Mosier, C. Krishnasamy, G. E. Kellogg, U. R. Desai, *PLoS One* **2012**, *7*, e48632.
- [12] a) H. Gerhardt, *Organogenesis* **2008**, *4*, 241; b) S. Wang, X. Li, M. Parra, E. Verdin, R. Bassel-Duby, E. N. Olson, *Proc. Natl. Acad. Sci. USA* **2008**, *105*, 7738.
- [13] a) S. Ashikari-Hada, H. Habuchi, Y. Kariya, K. Kimata, *J. Biol. Chem.* **2005**, *280*, 31508; b) A. M. Goodwin, *Microvasc. Res.* **2007**, *74*, 172; c) M. A. H. Lafleur, M. Madeleine, V. Knäuper, G. Murphy, D. R. Edward, *J. Cell Sci.* **2002**, *115*, 3427.
- [14] a) S. E. Sakiyama-Elbert, J. A. Hubbell, *J. Controlled Release* **2000**, *69*, 149; b) S. J. Taylor, J. W. McDonald, 3rd, S. E. Sakiyama-Elbert, *J. Controlled Release* **2004**, *98*, 281; c) K. Vulic, M. M. Pakulska, R. Sonthalia, A. Ramachandran, M. S. Shoichet, *J. Controlled Release* **2015**, *197*, 69.
- [15] a) Y. Shin, J. S. Jeon, S. Han, G. S. Jung, S. Shin, S. H. Lee, R. Sudo, R. D. Kamm, S. Chung, *Lab Chip* **2011**, *11*, 2175; b) A. Shamloo, H. Xu, S. Heilshorn, *Tissue Eng., Part A* **2012**, *18*, 320.
- [16] a) G. Marchioli, A. D. Luca, E. de Koning, M. Engelse, C. A. Van Blitterswijk, M. Karperien, A. A. Van Apeldoorn, L. Moroni, *Adv. Healthcare Mater.* **2016**, *5*, 1606; b) V. Moulisova, C. Gonzalez-Garcia, M. Cantini, A. Rodrigo-Navarro, J. Weaver, M. Costell, I. S. R. Sabater, M. J. Dalby, A. J. Garcia, M. Salmeron-Sanchez, *Biomaterials* **2017**, *126*, 61.
- [17] a) L. L. Chiu, M. Radisic, *Biomaterials* **2010**, *31*, 226; b) J. E. Leslie-Barbick, J. J. Moon, J. L. West, *J. Biomater. Sci., Polym. Ed.* **2009**, *20*, 1763.
- [18] M. M. Martino, P. S. Briquez, E. Guc, F. Tortelli, W. W. Kilarski, S. Metzger, J. J. Rice, G. A. Kuhn, R. Muller, M. A. Swartz, J. A. Hubbell, *Science* **2014**, *343*, 885.
- [19] a) L. Jakobsson, J. Kreuger, K. Holmborn, L. Lundin, I. Eriksson, L. Kjellen, L. Claesson-Welsh, *Dev. Cell* **2006**, *10*, 625; b) L. Schirmer, P. Atallah, C. Werner, U. Freudenberg, *Adv. Healthcare Mater.* **2016**,

- 5, 3157; c) M. Teran, M. A. Nugent, *J. Biol. Chem.* **2015**, *290*, 16451; d) E. Wijelath, M. Namekata, J. Murray, M. Furuyashiki, S. Zhang, D. Coan, M. Wakao, R. B. Harris, Y. Suda, L. Wang, M. Sobel, *J. Cell. Biochem.* **2010**, *111*, 461.
- [20] K. Ono, H. Hattori, S. Takeshita, A. Kurita, M. Ishihara, *Glycobiology* **1999**, *9*, 705.
- [21] U. Freudenberg, J.-U. Sommer, K. R. Levental, P. B. Welzel, A. Zieris, K. Chwalek, K. Schneider, S. Prokoph, M. Prewitz, R. Dockhorn, C. Werner, *Adv. Funct. Mater.* **2012**, *22*, 1391.
- [22] A. K. Jha, A. Mathur, F. L. Svedlund, J. Ye, Y. Yeghiazarians, K. E. Healy, *J. Controlled Release* **2015**, *209*, 308.
- [23] D. B. Pike, S. Cai, K. R. Pomraning, M. A. Firpo, R. J. Fisher, X. Z. Shu, G. D. Prestwich, R. A. Peattie, *Biomaterials* **2006**, *27*, 5242.
- [24] K. Guzik, J. Potempa, *Biochimie* **2008**, *90*, 405.
- [25] U. Freudenberg, Y. Liang, K. L. Kiick, C. Werner, *Adv. Mater.* **2016**, *28*, 8861.
- [26] S. Rother, S. A. Samsonov, S. Moeller, M. Schnabelrauch, J. Rademann, J. Blaszkiewicz, S. Kohling, J. Waltenberger, M. T. Pisabarro, D. Scharnweber, V. Hintze, *ACS Appl. Mater. Interfaces* **2017**, *9*, 9539.
- [27] a) B. M. Loo, J. Kreuger, M. Jalkanen, U. Lindahl, M. Salmivirta, *J. Biol. Chem.* **2001**, *276*, 16868; b) S. Roy, H. Lai, R. Zouaoui, J. Duffner, H. Zhou, P. J. L. G. Zhao, T. Ganguly, T. K. Kishimoto, G. Venkataraman, *Glycobiology* **2011**, *21*, 1194; c) R. Sadir, F. Baleux, A. Grosdidier, A. Imberty, H. Lortat-Jacob, *J. Biol. Chem.* **2001**, *276*, 8288; d) R. A. A. Smith, S. Murali, B. Rai, X. Lu, Z. X. H. Lim, J. J. L. Lee, V. Nurcombe, S. M. Cool, *Biomaterials* **2018**, *184*, 41; e) W. Zhao, S. A. McCallum, Z. Xiao, F. Zhang, R. J. Linhardt, *Biosci. Rep.* **2012**, *32*, 71.
- [28] a) M. H. Hettiaratchi, T. Rouse, C. Chou, L. Krishnan, H. Y. Stevens, M. A. Li, T. C. McDevitt, R. E. Gulberg, *Acta Biomater.* **2017**, *59*, 21; b) D. J. Maxwell, B. C. Hicks, S. Parsons, S. E. Sakiyama-Elbert, *Acta Biomater.* **2005**, *1*, 101.
- [29] M. V. Galanternik, K. L. Kramer, T. Piotrowski, *Cell Rep.* **2015**, *10*, 414.
- [30] S. P. Seto, T. Miller, J. S. Temenoff, *Bioconjugate Chem.* **2015**, *26*, 286.
- [31] a) G. S. Jeong, S. Han, Y. Shin, G. H. Kwon, R. D. Kamm, S. H. Lee, S. Chung, *Anal. Chem.* **2011**, *83*, 8454; b) B. Trappmann, B. M. Baker, W. J. Polacheck, C. K. Choi, J. A. Burdick, C. S. Chen, *Nat. Commun.* **2017**, *8*, 371; c) J. A. Whisler, M. B. Chen, R. D. Kamm, *Tissue Eng., Part C* **2014**, *20*, 543.
- [32] D. Hanjaya-Putra, K. T. Wong, K. Hirotsu, S. Khetan, J. A. Burdick, S. Gerecht, *Biomaterials* **2012**, *33*, 6123.
- [33] A. Farrukh, J. I. Paez, A. del Campo, *Adv. Funct. Mater.* **2018**, *29*.
- [34] a) J. Grunstein, J. J. Masbad, R. Hickey, F. Giordano, R. S. Johnson, *Mol. Cell. Biol.* **2000**, *20*, 7282; b) J. E. Park, G. A. Keller, N. Ferrara, *Mol. Biol. Cell* **1993**, *4*, 1317.
- [35] a) Y. Tabata, M. P. Lutolf, *Sci. Rep.* **2017**, *7*, 44711; b) S. G. Uzel, O. C. Amadi, T. M. Pearl, R. T. Lee, P. T. So, R. D. Kamm, *Small* **2016**, *12*, 612.
- [36] a) C. J. Wienken, P. Baaske, U. Rothbauer, D. Braun, S. Dühr, *Nat. Commun.* **2010**, *1*, 100; b) S. A. Seidel, P. M. Dijkman, W. A. Lea, G. van den Bogaart, M. Jerabek-Willemsen, A. Lazic, J. S. Joseph, P. Srinivasan, P. Baaske, A. Simeonov, I. Katritch, F. A. Melo, J. E. Ladbury, G. Schreiber, A. Watts, D. Braun, S. Dühr, *Methods* **2013**, *59*, 301.
- [37] F. Brandl, F. Kastner, R. M. Gschwind, T. Blunk, J. Teßmar, A. Göpferich, *J. Controlled Release* **2010**, *142*, 221.
- [38] D. M. Soumpasis, *Biophys. J.* **1983**, *41*, 95.
- [39] I. K. Zervantonakis, S. K. Hughes-Alford, J. L. Charest, J. S. Condeelis, F. B. Gertler, R. D. Kamm, *Proc. Natl. Acad. Sci. USA* **2012**, *109*, 13515.
- [40] J. R. Weis, B. Sun, G. M. Rodgers, *Thromb. Res.* **1991**, *61*, 171.